Supplementary Material (ESI) for Chemical Communications

Single molecule magnet behaviour in robust Dysprosium-biradical complexes

Kevin Bernot,*[a,b] Fabrice Pointillart,[a] Patrick Rosa,[c] Maël Etienne[a], Roberta Sessoli[a*] and Dante Gatteschi[a]

[a]L.A.M.M, department of chemistry and INSTM Reasearch Unit, Università di Firenze, Via Della Lastruccia 3, 50019 Sesto Fiorentino (FI) Italy. Fax: +39-55-4573372; Tel: +39-55-4573268; E-mail: roberta.sessoli@unifi.it.
[b] Université Européenne de Bretagne, France
INSA, SCR, UMR 6226, F-35708 RENNES
Fax: +33-(0)2 23238606; Tel: +33-(0)2 23238482;E-Mail : kevin.bernot@insa-rennes.fr.
[c]CNRS, Universite de Bordeaux, ICMCB, 87 Av. Doc. A. Schweitzer,F- 33608 Pessac (France).

Experimental procedure. On one hand 0.05 mmol (19.4 mg) of NITmbis is dissolved in 5 ml of $CHCl_3$. On the other hand, 0.05 mmol (41 mg) of $Dy(hfac)_3 \cdot 2H_2O$ ($hfac^-$ = 1,1,1,5,5,5-hexafluoroacetylacetonate)[1] is dissolved in 5 ml of $CHCl_3$. Both solutions are poured simultaneously in a 15 ml hot heptane solution. After some days of slow evaporation, deep-blue prismatic crystals of $[Dy(hfac)_3(NITmbis)]_2$ (noted **DyNITmbis**) appears and are suitable for X-Ray diffraction.

Physical measurements. Crystals were selectioned and then frozen at T = 150 K under a stream of dry N_2 on a APEXII Bruker-AXS diffractometer for data collection (Mo-K_α radiation, λ = 0.71073 Å). Data reduction was accomplished using SADABS program. Absorption correction were applied. Structure was solved by direct methods (SIR97)[2] and refined (SHELXL 97)[3] by full-matrix least-squares methods as implemented in the WinGX sofware package.[4] Hydrogen atoms were introduced at calculated positions (riding model) included in structure factor calculations but not refined. The two $hfac^-$ anions that involve the O5, O6, O7 and O8 oxygen atoms are disordered in two positions. The occupation factors are approximatly 0.80 and 0.20. Nevertheless the refinment is not stable when the disorder is taken into account. However it do not hampers the interpretation of the magnetic behavior of the compound that is the main concern of this paper. Consequently the structure was solved without considering this disorder.

Solid-state and solution absorption spectra were recorded using respectively the KBr disk method and solutions of both species in CH_2Cl_2 ($c = 5.10^{-5}$ mol L^{-1}) on a varian Cary 5000 UV-visible-NIR spectrometer equipped with an integration sphere. X-band EPR spectra were measured on a Bruker Elexsys E500 spectrometer. The *dc*-magnetic susceptibility measurements were performed on solid polycrystalline samples with a Cryogenic S600 SQUID magnetometer between 2 and 300 K in applied magnetic field of 100 Oe for temperatures of 2-65 K 1 kOe for temperatures of 65-250 K and 10 kOe for temperatures of 250-300 K. These measurements were all corrected for the diamagnetic contribution as calculated with Pascal's constants. The *ac*-magnetic susceptibility measurements were performed using a homemade probe operating in the range 100-25000 Hz.[3] Sub-kelvin AC susceptibility measurements were performed on a modified Oxford Instruments ^{3}He Heliox cryostat, and a homemade AC probe by courtesy of Prof. M. Novak (UFRJ, Rio de Janeiro, Brazil): available temperature range 280–2000 mK, frequency range 20–15000 Hz, for oscillating field excitations up to 0.33 Oe. All measurements were performed on pellets in order to avoid orientation of the microcrystals of this very anisotropic material.

1 Richardson, M. F.; Wagner, W. F.; Sands, D. E. *J. Inorg. Nucl. Chem.* **1968**, *30*, 1275.
2 Altomare, A.; Cascarano, G.; Giacovazzo, C.; Guagliardi, A.; Burla, M. C.; Polidori, G.; Camalli, M. *J. Apll. Crystallogr.* **1994**, *27*, 435.
3 G. M. Sheldrick, SHELXL-97, Program for refinement of crystal structures, University of Göttingen, Germany, **1997**.
4 Farrugia, L. J. *J. appl. Crystallogr.* **1999**, *32*, 837.
5 S. Midollini, A. Orlandini, P. Rosa, L. Sorace, *Inorg. Chem.* **2005**, *44*, 2060.

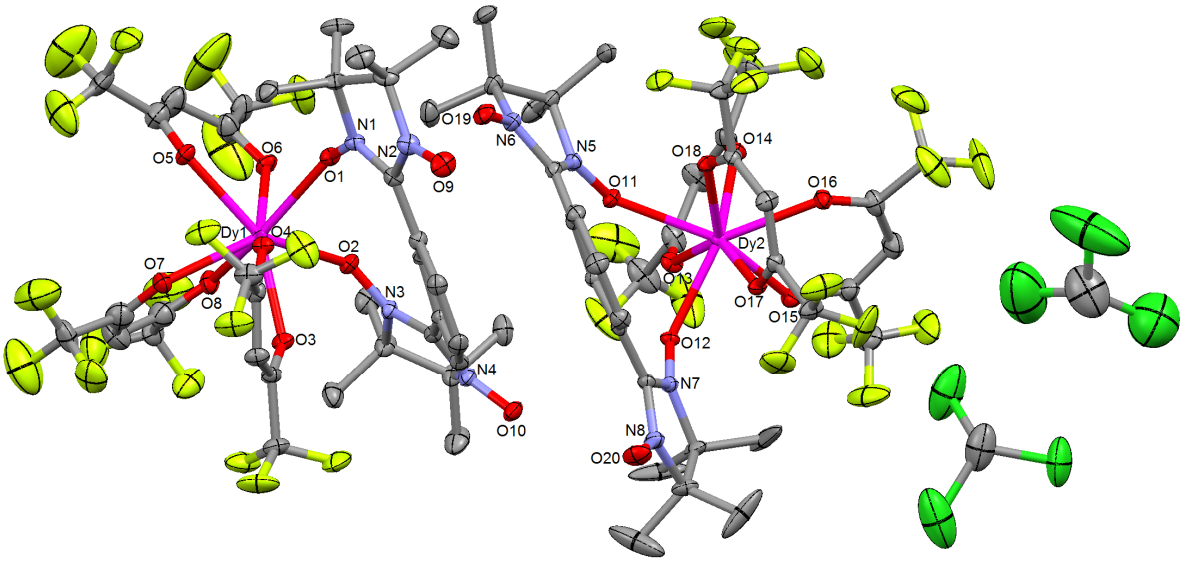

Figure S1. ORTEP view of the asymmetric unit of **DyNIT*m*bis** with thermal ellipsoids at 30% probability. Hydrogen atoms are omitted for clarity.

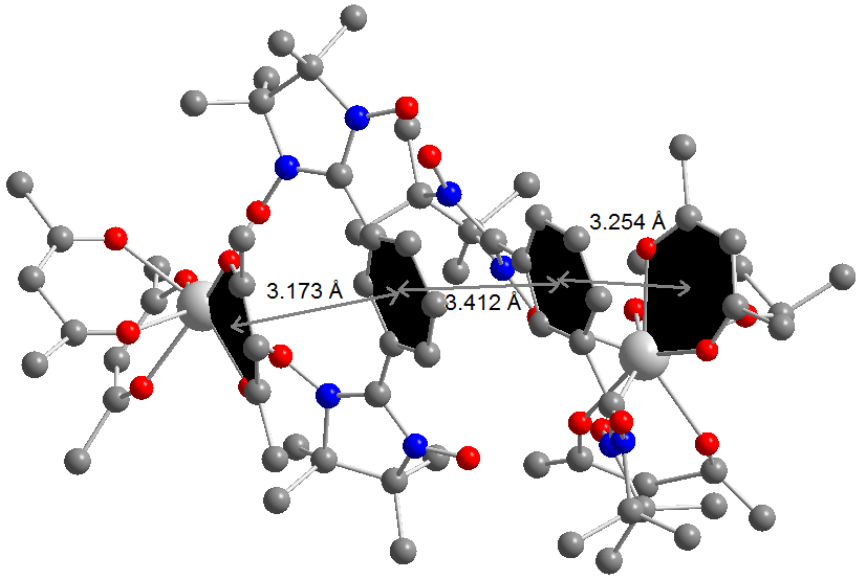

Figure S2. Schematic view of the packing of two **DyNIT*m*bis** units highlighting the π-π interactions between the aromatic systems of the $hfac^-$ ligands and phenyl groups. The distances which are given correspond to the shortest distances between two atoms.

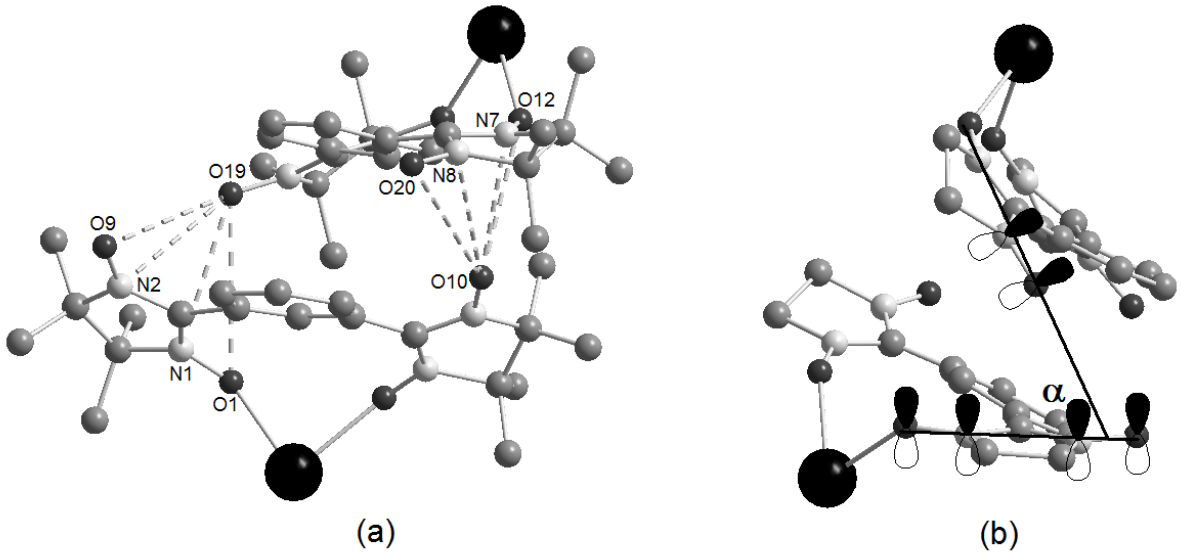

Figure S3. (a) Schematic view of the interactions between the free N_i-O19 and N_i-O10 groups with the O9-N2-C-N1-O1 and O20-N8-C-N7-O12 systems. The O19-O9, O19-N2, O19-N1, O19-O1, O10-O20, O10-N8, O10-N7 and O10-O12 distances are equal to 4.391(6), 3.648(6), 3.088(5), 3.365(5), 4.706(7), 3.289(6), 3.374(5) and 3.897(5) Å respectively. (b) Highlight of the α angle (79.4°) between the two planes containing the π radical orbitals.

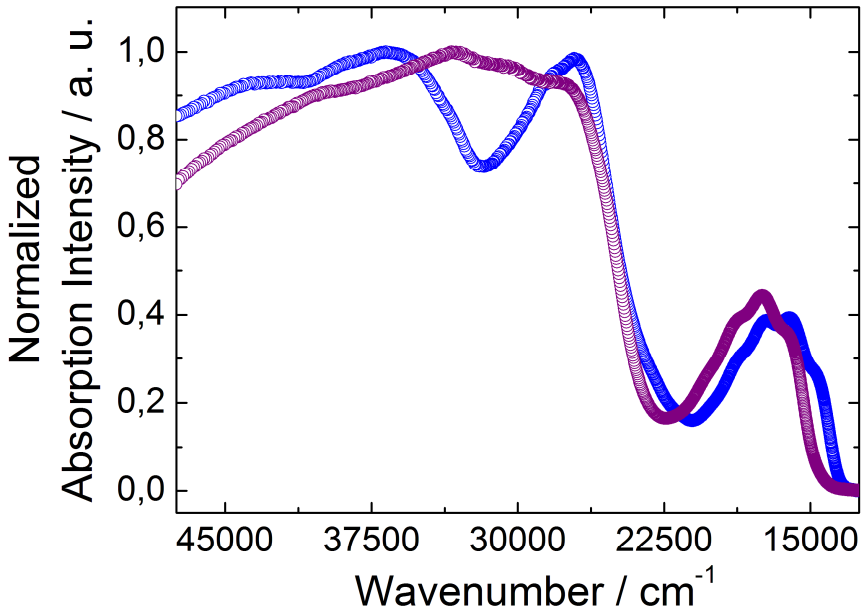

Figure S4. Experimental solid-state UV-visible absorption spectra of NITmbis (blue open circles) and **DyNIT*m*bis** (purple open circles).

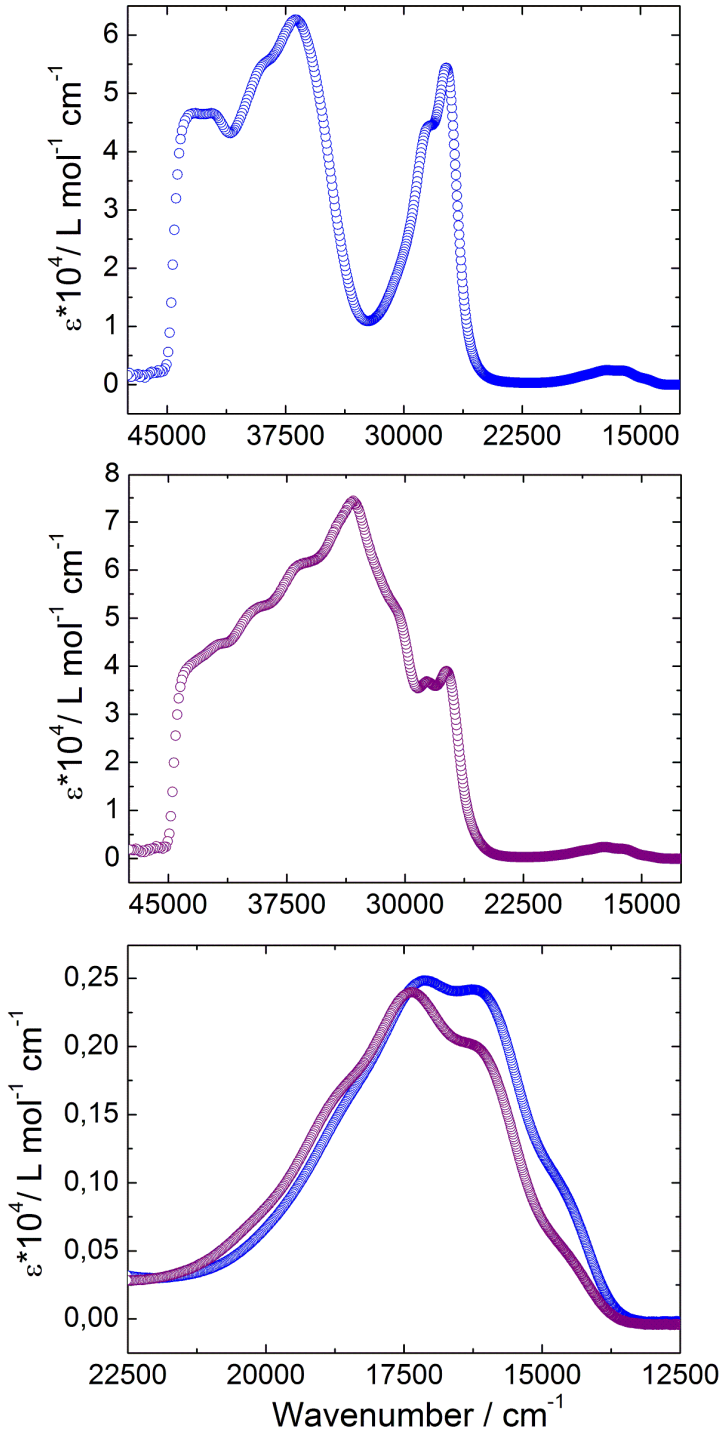

Figure S5. Experimental UV-visible absorption spectra of NITmbis (top) and **DyNIT*m*bis** (center) in CH_2Cl_2 ($c = 5.10^{-5}$ mol.L^{-1}) at room temperature. Zoom of the charge transfer region for both species highlighting the change of shape of the curves and the blue shift (bottom).

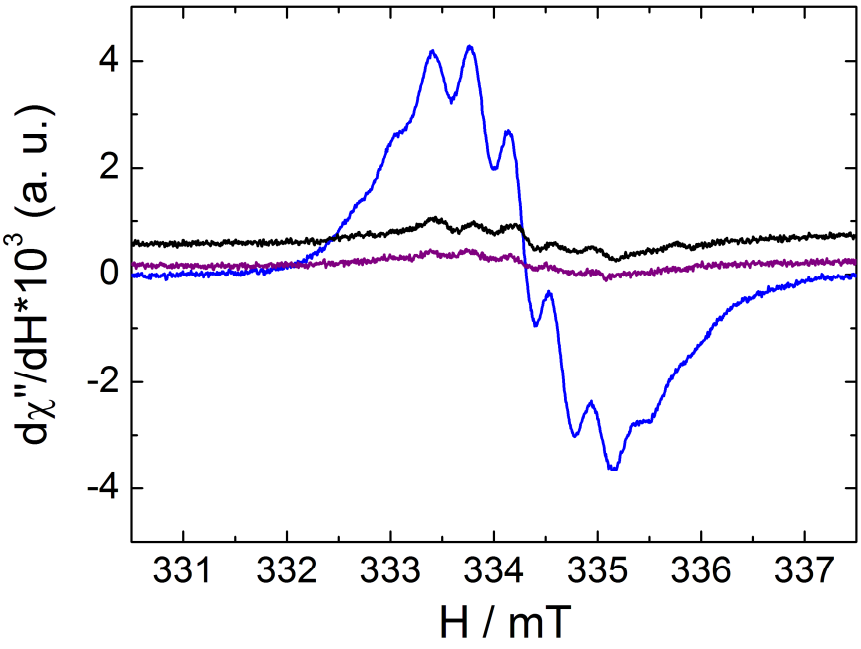

Figure S6. X-Band (9.364 GHz) EPR spectra of NITmbis (blue line), **DyNIT*m*bis** (purple line) and two days aged **DyNIT*m*bis** CH_2Cl_2 solution (black line). All solutions are equimolar.

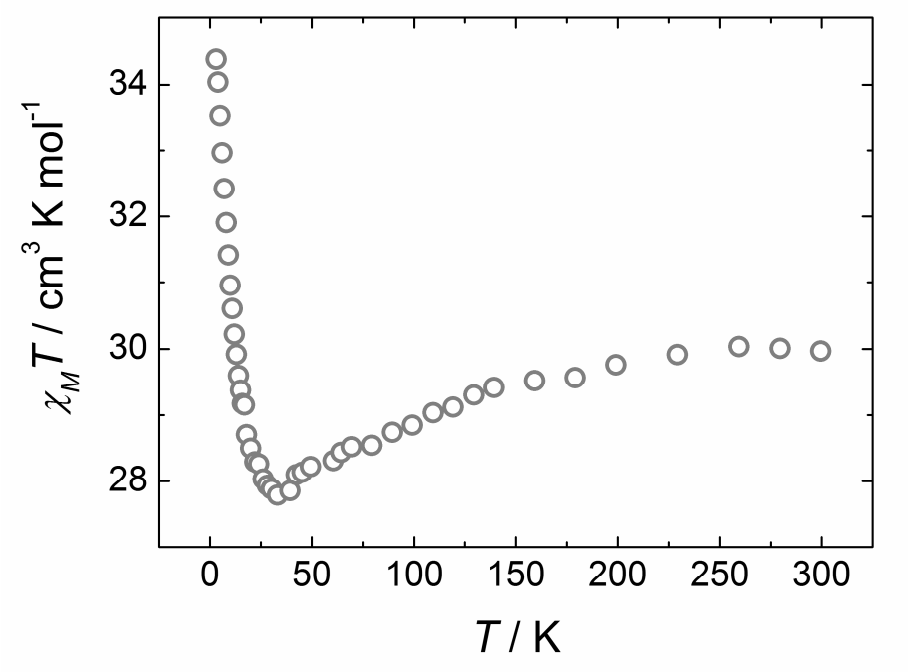

Figure S7. Temperature dependence of the $\chi_M T$ product from dc magnetic measurements for **DyNITmbis** (open gray circles).

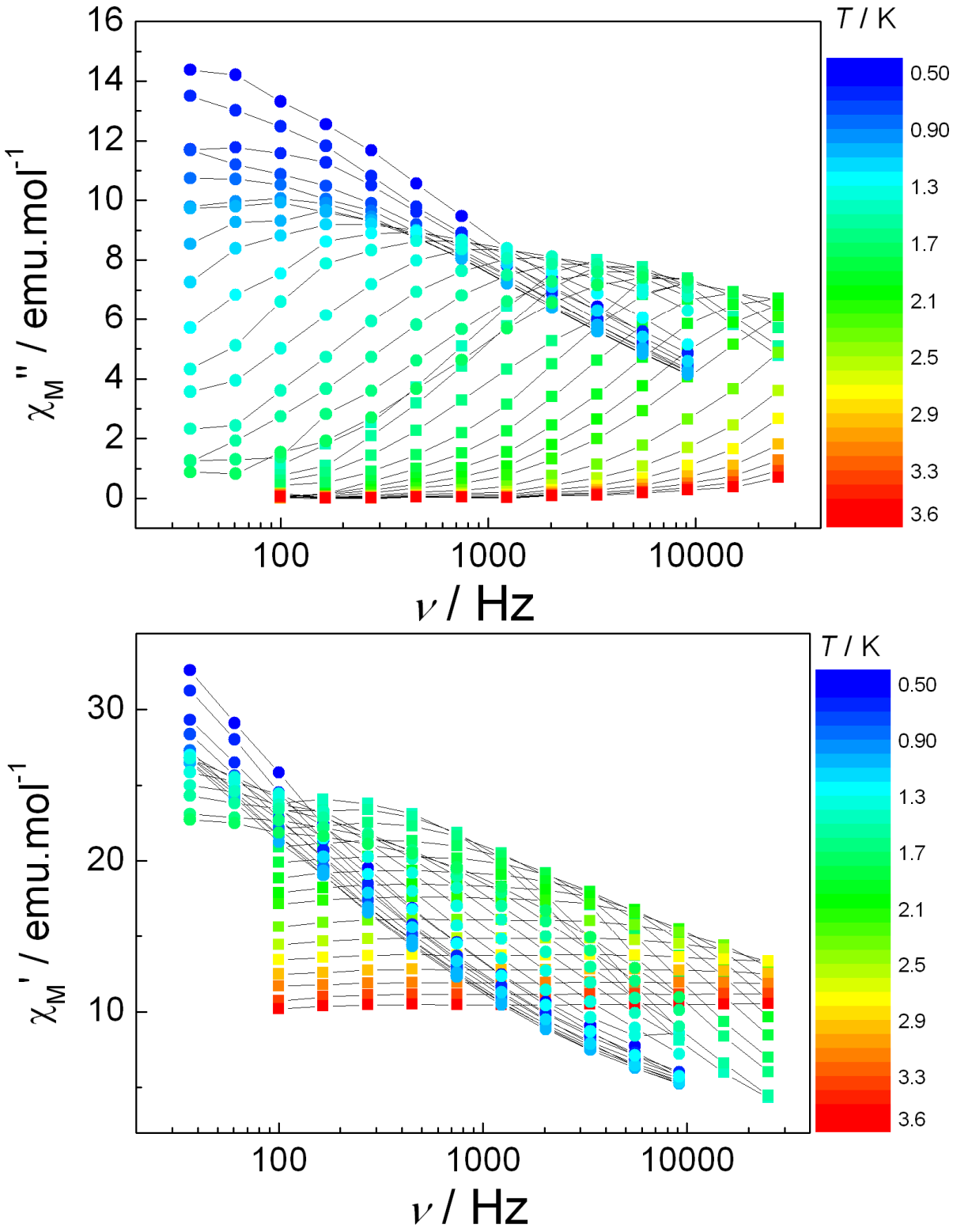

Figure S8. Frequency dependence of the in-phase and out-of-phase susceptibility measured in the 0.5-3.7 K temperature range on 15 logarithmic-spaced frequencies. From 0.5K to 1.72 K a ^{3}He-cooled cryostat was used, 36-9161Hz (circles). From 1.55K to 3.6K a ^{4}He-cooled cryostat was used, 100-25000Hz (squares).

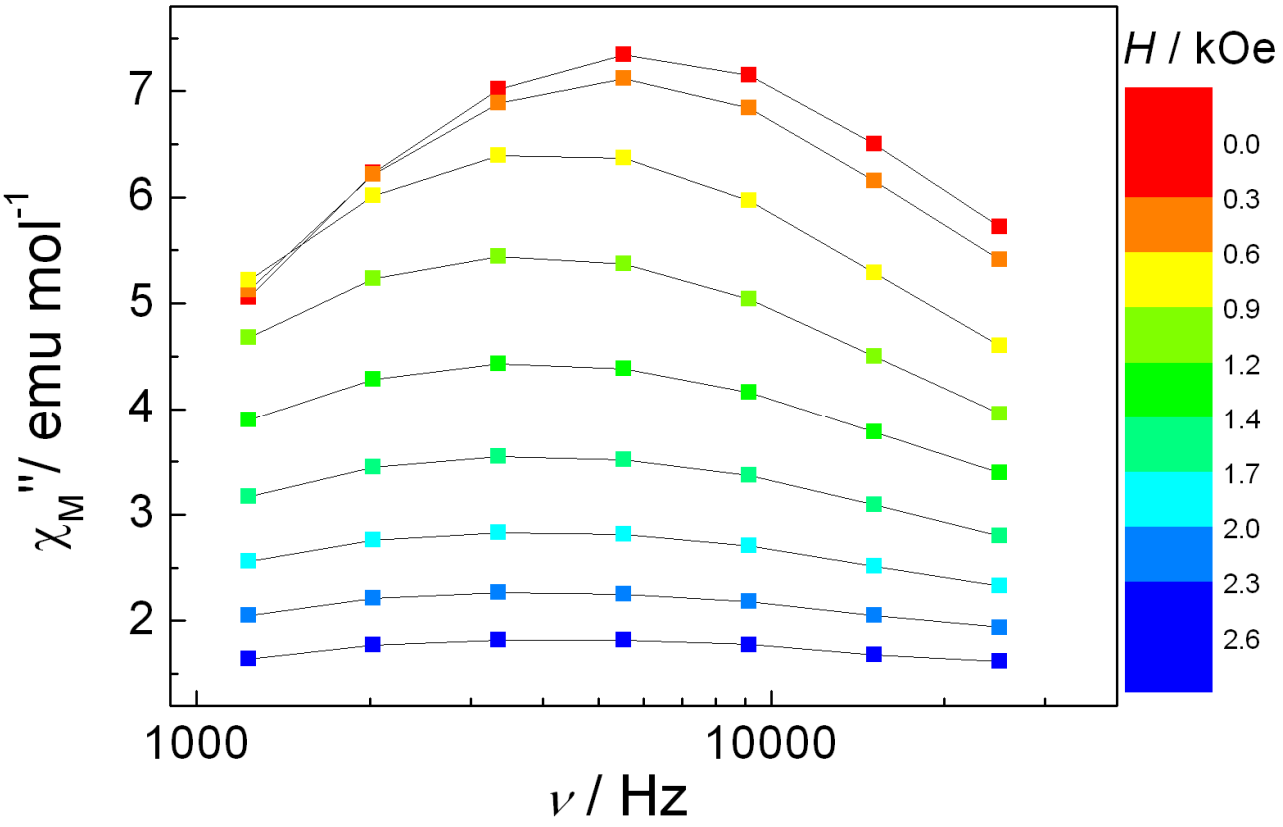

Figure S9. Field dependence of the out-of-phase susceptibility, at 1.65 K, in a 0-3 kOe range using 7 logarithmic-spaced frequencies (1200-25000 Hz).

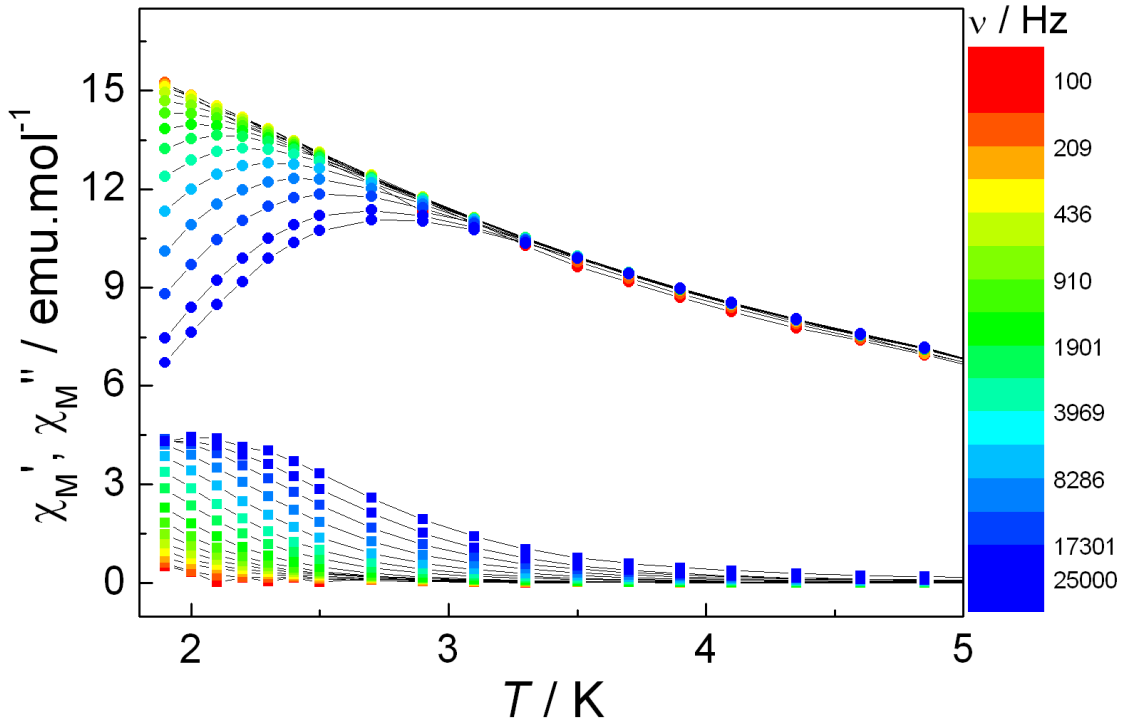

Figure S10. Temperature dependence of the in-phase (circles) and out-of-phase (squares) susceptibility measured in the 1.5-5K temperature range with 15 logarithmic-spaced frequencies (100-25000Hz) in a 1 kOe external field.

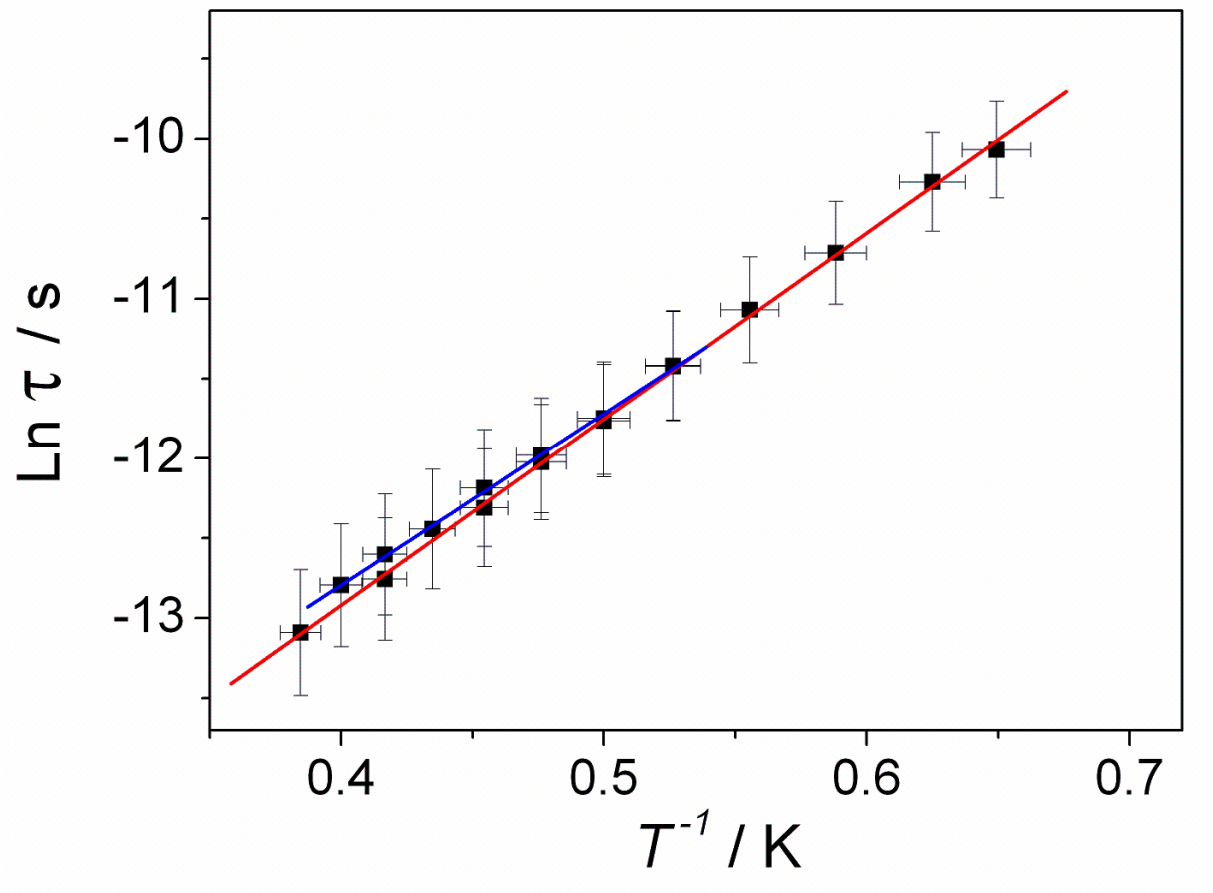

Figure S11. Temperature dependence of the relaxation time (logarithmic) as extracted from the out-of-phase susceptibility measured without (square, red line as best fit) or with a 0.1 kOe external field (circles, blue line as best fit). Data are fitted with an Arrhenius law, parameters can be found in the text.

Table S1. Selected bond lengths for **DyNITmbis**

	DyNITmbis
Dy(1)-O(1)	2.392(4)
Dy(1)-O(2)	2.380(4)
Dy(1)-O(3)	2.332(4)
Dy(1)-O(4)	2.377(4)
Dy(1)-O(5)	2.336(4)
Dy(1)-O(6)	2.384(4)
Dy(1)-O(7)	2.373(4)
Dy(1)-O(8)	2.356(4)
Dy(2)-O(11)	2.418(4)
Dy(2)-O(12)	2.350(4)
Dy(2)-O(13)	2.359(4)
Dy(2)-O(14)	2.330(4)
Dy(2)-O(15)	2.324(4)
Dy(2)-O(16)	2.366(4)
Dy(2)-O(17)	2.369(4)
Dy(2)-O(18)	2.327(4)

Table S2. Main fitting parameters for the Argand plot.

T(K)	χ_T	α	R^2	T(K)	χ_T	α	R^2
0.52	72.73	0.50	0.99943	1.32	29.71	0.27	0.97887
0.6	73.76	0.54	0.99947	1.40	28.08	0.26	0.99369
0.68	54.41	0.48	0.99911	1.48	25.96	0.22	0.99043
0.76	57.50	0.51	0.99842	1.50	25.14	0.24	0.97046
0.84	51.13	0.48	0.99960	1.56	24.75	0.20	0.99850
0.92	44.63	0.48	0.99947	1.60	24.67	0.25	0.9617
1	44.35	0.45	0.99936	1.64	23.25	0.16	0.99653
1.08	39.00	0.40	0.99785	1.70	23.50	0.26	0.95233
1.16	35.72	0.37	0.99640	1.72	22.72	0.23	0.99501
1.24	32.43	0.34	0.98960				